NANO · MICRO small
www.small-journal.com

Synthesis of Silver Nanoparticles from Silver Closo-Dodecaborate Film for Enhanced Hydrogen Evolution

*Majharul Haque Khan, Chao Han, Xuefei Wang, Weijie Li, Guojin Zhang, and Zhenguo Huang**

The icosahedral *closo* dodecaborate cluster $[B_{12}H_{12}]^{2-}$ is gaining increasing interest due to its unique properties including the ease of functionalization, 3D aromaticity, and formation of metal salts with high ion conductivity. In this work, simple and effective preparation of silver *closo* dodecaborte ($Ag_2B_{12}H_{12}$) films is reported by an electrochemical route. The size of the $Ag_2B_{12}H_{12}$ particles in the films can be tuned from nanometers to micrometers by varying the electrochemical parameters. Ag nanoclusters with controllable sizes are successfully generated via electrochemical reduction reactions or thermal anneal of the $Ag_2B_{12}H_{12}$ films. When tested for hydrogen evolution reaction (HER) in an acidic solution, the as-prepared Ag nanoparticles deliver a current density of 10 mA cm^{-2} at 376 mV overpotential. This research sheds light on a new synthesis of $[B_{12}H_{12}]^{2-}$ based thin films, the generation of metal nano-powders, and their application in HER or other applications.

1. Introduction

Novel and effective synthesis is critical in developing materials with the desired properties for applications in catalysis, batteries, and electronics. For example, a myriad of innovative syntheses have been developed to fabricate high-performance and cost-effective catalysts for hydrogen evolution reaction (HER) via water electrolysis.[1–7] HER has been considered the most sustainable way of generating hydrogen in large quantities. In commercial polymer electrolyte membrane (PEM) electrolyzers, Pt is the primary choice of catalyst for HER. To reduce CO_2 emissionandaddress climate change, substantially larger electrolyzers are needed. The earth has limited Pt reserve, and therefore alternative catalysts have been explored. Compared with the commercial Pt-based HER catalyst, Ag is more abundant and highly conductive, and therefore has been explored as an alternative electrocatalyst.[8–14] Various methods have been developed to reduce the size,[8,9,11,13] tune the morphology[15,16] and generate defects[13] of Ag nanoparticles to enhance its HER performance.[11] Among these, size reduction is especially effective in increasing the number of active sites that in turn dramatically improve the performance. For example, nanoporous Ag foam[15] and Ag nanodendrite films[16] showed higher HER performance than the polycrystalline Ag foil. However, the complexity in the syntheses of Ag nanoparticles, the lack of control of size and shape, and poor reproducibility, limit the utilization of the full potentials of Ag nanoparticles.[17]

The large *closo*-dodecaborate anion $[B_{12}H_{12}]^{2-}$ is drawing increasing interest in the field of boron chemistry recently. Due to the 3D aromaticity of the anion,[18–20] the negative charge is distributed over 12 hydrides in a large sphere, resulting in weak columbic interactions with metal counter cation. This likely enables fast Ag nanofilament growth from $Ag_2B_{12}H_{12}$ under high energy electron beam in transmission electron microscopes.[21] This motivates us to investigate the formation of Ag nanoparticles from $Ag_2B_{12}H_{12}$ by carrying out electrochemical reduction reactions. We expect a controllable growth of Ag nanoparticles considering the weak interactions between Ag^+ ions and the large spherical $[B_{12}H_{12}]^{2-}$ anions that can facilitate Ag^+ ion reduction and steady supply of Ag^+ ion during the process.[22,23]

In this work, a new and effective electrochemical synthesis of $Ag_2B_{12}H_{12}$ film on Ag foil was first developed. By varying the parameters, the $Ag_2B_{12}H_{12}$ particle size in the films can be controllably varied from nanometer to micrometer. When $Ag_2B_{12}H_{12}$ film on Ag was used as a working electrode, Ag^+ ion reduction to Ag (0) was achieved resulting in uniform Ag nanoparticles, which displayed high HER activity that is significantly better than the bare Ag substrate. This in situ metallic nanoparticle generation

M. H. Khan, X. Wang, G. Zhang, Z. Huang
School of Civil and Environmental Engineering
University of Technology Sydney
Sydney, NSW 2007, Australia
E-mail: zhenguo.huang@uts.edu.au

C. Han
School of Materials Science and Engineering
Central South University
Hunan 410083, P. R. China

C. Han, W. Li
Powder Metallurgy Research Institute
Central South University
Hunan 410083, P. R. China

The ORCID identification number(s) for the author(s) of this article can be found under https://doi.org/10.1002/smll.202305117

DOI: 10.1002/smll.202305117

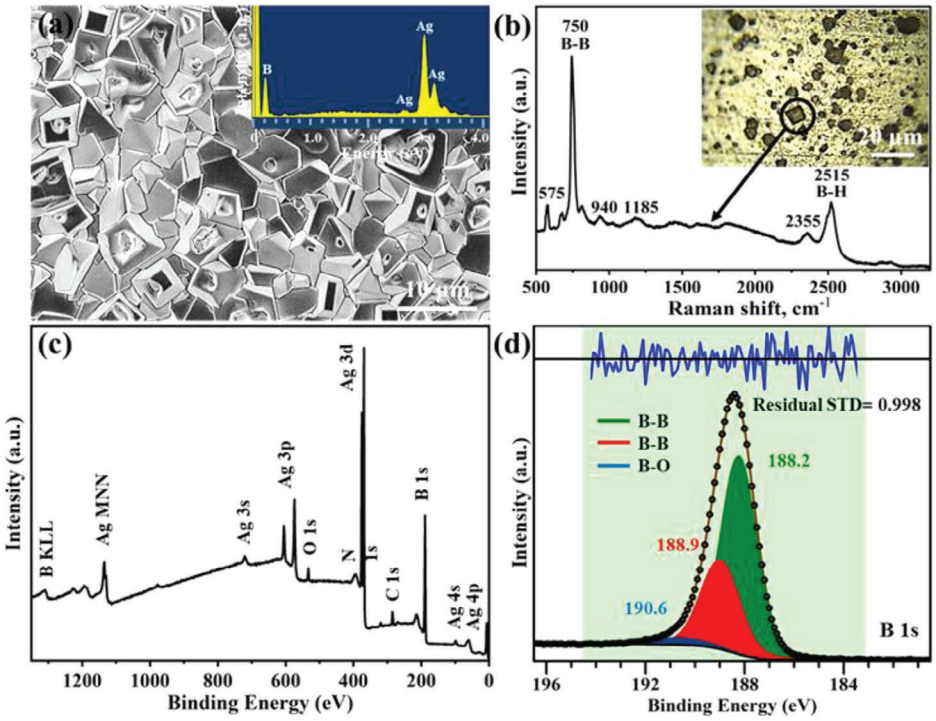

Figure 1. a) Electrochemical synthesis of $Ag_2B_{12}H_{12}$ film on a Ag foil with representative EDX analysis shown in the inset; b) Raman analysis on a $Ag_2B_{12}H_{12}$ particle (the optical image shown in the inset) confirms the characteristic B—H and B—B bond of a $[B_{12}H_{12}]^{2-}$ cluster; c) XPS survey spectrum of the $Ag_2B_{12}H_{12}$ film on a Ag foil; d) XPS B 1s spectrum shows three peaks, with peaks at 188.2 and 188.9 eV assigned to B—B, peak at 190.6 eV to B—O.

from the metal *closo* dodecaborate compounds can be potentially employed to obtain other metal nanoparticles.

2. Results and Discussion

2.1. Synthesis of $Ag_2B_{12}H_{12}$ Film and its Characterizations

Electrochemical synthesis of $Ag_2B_{12}H_{12}$ film was carried out on clean Ag foils using a standard three-electrode cell setup (details in the supplementary information). The current and voltage were regulated via a CHI electrochemical workstation. 20 mmol $Na_2B_{12}H_{12}$ solution in water (pH ≈6) was used as the analyte. Under a specific voltage, Ag^+ ions were generated from the Ag foil working electrode. At the same time, $[B_{12}H_{12}]^{2-}$ anions from the solution were attracted to the Ag working electrode under the applied voltage and combined with the as-produced Ag^+ ions. Ag foils covered completely with a grey-colored $Ag_2B_{12}H_{12}$ film was achieved at 0.84 V (versus a reversible hydrogen electrode (RHE)) after 10 min. The thickness of the film is ≈3 μm, determined using a profilometer (Figure S1, Supporting Information). Subsequently, the samples were analyzed under the scanning electron microscope (SEM) and energy dispersive X-ray (EDX). Analyzing the SEM images with a Fiji ImageJ software, the mean crystallite size was estimated to be ≈6.4 μm (**Figure 1**a). Most $Ag_2B_{12}H_{12}$ crystallites appear to be octahedrons. The EDX analysis indicated the presence of only Ag and B in the particles (inset of Figure 1a).

Further characterization of the sample was carried out by Raman spectroscopy, Fourier Transformed Infrared Spectroscopy (FTIR), X-ray photoelectron spectroscopy (XPS), and X-ray diffraction (XRD). Raman spectrum indicates the presence of B—H stretching bond at 2515 and 2355 cm^{-1} (Figure 1b).[24,25] The peak at 2355 cm^{-1} could be either due to the strain-induced slight B—H bond elongation inside the borane cluster in the presence of Ag ions[25] or Ag-B—H bridging bond formation.[26] The strain in the cluster may also contribute to the 575 cm^{-1} (B-B-B deformation mode) Raman peak. [24,27–29] The prominent peak at 750 cm^{-1} can be assigned to the B—B bending vibrations. This confirms the presence of $Ag_2B_{12}H_{12}$ formation on the Ag surface (Figure 1c). Also, the FTIR spectrum collected on the deposited area reveals B—H stretching, B-H bending, and B-B bending vibration (Figure S2, Supporting Information). Contrast to the common hydrated *closo* dodecaborates, water IR peaks are invisible in the FTIR spectrum.[30] All these results confirm that $Ag_2B_{12}H_{12}$ has formed during the electrochemical process. The XPS peaks of carbon, oxygen, and nitrogen in the survey spectrum are due to the exposure of the sample to air during handling. Notably, Na is invisible in the spectrum. Three peaks, centered at 188.2, 188.9 and 190.01 eV can be identified after the deconvolution of the B 1s peak, indicating three different chemical environments for boron atoms. Both peaks at 188.2 and 188.9 eV can be assigned to the B-B peaks.[31–33] The formation of two peaks is due to the polarization of $[B_{12}H_{12}]^{2-}$ toward the Ag^+ ions, leading to different B—B bond lengths inside the cluster.[34] The minor peak at 190.6 eV is associated with the B—O bonds.[31]

Electrochemical syntheses of $Ag_2B_{12}H_{12}$ were also carried out under various parameters, i.e., voltage, current density,

concentration of $Na_2B_{12}H_{12}$ solution, and time, to control the growth of $Ag_2B_{12}H_{12}$ on Ag surface (Figure S3, Supporting Information). At a low voltage (<0.79 V vs RHE), $Ag_2B_{12}H_{12}$ did not form on Ag. At 0.81 V, discrete $Ag_2B_{12}H_{12}$ particles were found on Ag surface after 10 min. A continuous $Ag_2B_{12}H_{12}$ film was only seen at 0.84 V after 10 min. Below 10 min, only islands of $Ag_2B_{12}H_{12}$ were obtained. At higher voltages (> 0.9 V vs RHE), 1 min was sufficient to achieve complete coverage with small crystallites (≈1 μm). Increasing the growth duration to 10 min did not notably enlarge the size of the crystallites. In the subsequent runs, we then fixed the time of growth to 1 min and changed the other parameters. However, using $Na_2B_{12}H_{12}$ with concentrations of 5 and 10 mM at a fixed 0.9 V vs RHE resulted in only a partially $Ag_2B_{12}H_{12}$ covered Ag surface after 1 min. On the other hand, increasing the current density from 1 to 5 mA cm^{-2} or higher (10 mA cm^{-2}), with a 20 mM $Na_2B_{12}H_{12}$ solution, a complete coverage was obtained within 1 min, with a mean $Ag_2B_{12}H_{12}$ particle size of only ≈500 nm (Figure S3k, Supporting Information).

The mechanism of $Ag_2B_{12}H_{12}$ formation on the Ag surface can be explained as follows. The redox potential for Ag to Ag^+ is 0.7995 V vs RHE, which means that above this voltage Ag^+ starts to form at the Ag foil surface. In the $Na_2B_{12}H_{12}$ aqueous solution, the positive Ag^+ ions will attract the $[B_{12}H_{12}]^{2-}$ anions toward the Ag surface, forming insoluble $Ag_2B_{12}H_{12}$ on the Ag foil. As can be seen from Figure S2 (Supporting Information), $Ag_2B_{12}H_{12}$ did not form below 0.79 V vs RHE. At 0.81 V vs RHE, the rate of Ag^+ ion formation is slow and can be considered as the rate-limiting step. Thus, only islands of $Ag_2B_{12}H_{12}$ on top of the Ag surface were found after 10 min. At 0.84 V vs RHE, we saw large $Ag_2B_{12}H_{12}$ crystallites (5–10 μm) and complete coverage of the Ag surface after 10 min. Once complete coverage is achieved, a further increase in growth time does not make any significant change in the $Ag_2B_{12}H_{12}$ particle size. Rapid nucleation and growth were also observed when the current density was increased to 5 and 10 mA cm^{-2}. The concentration of $Na_2B_{12}H_{12}$ also affects the growth rate of $Ag_2B_{12}H_{12}$. At least 20 mM $Na_2B_{12}H_{12}$ was needed to get a complete coverage of the Ag surface with $Ag_2B_{12}H_{12}$, under the above-mentioned potential and reaction time; while only partial coverage was achieved at low concentrations (5 and 10 mM, Figure S3d,e, Supporting Information).

When a complete coverage of the Ag foil surface was achieved, especially at 0.84 V vs RHE after 10 min (Figure S3c, Supporting Information), holes were visible on the $Ag_2B_{12}H_{12}$ particles. For $Ag_2B_{12}H_{12}$ formed on a partially covered Ag foil surface, holes were barely seen. This could be due to the limited mobility and supply of Ag^+ ions once closely packed $Ag_2B_{12}H_{12}$ particles are formed. Nevertheless, the Ag surface can be completely covered by $Ag_2B_{12}H_{12}$ particles under the optimum conditions discussed above.

2.2. HER Analysis of $Ag_2B_{12}H_{12}$ Films on Ag Foils

The linear sweep voltammetry (LSV) polarization curves of the synthesized $Ag_2B_{12}H_{12}$ films on Ag foils (synthesized at 0.84 V vs RHE for 10 min, in 20 mM $Na_2B_{12}H_{12}$ solution) in 0.5 M H_2SO_4 solution are shown in **Figure 2**a. As can be seen from the LSV curves, the material displayed a decent HER performance, even after several hours of testing. A current density of 10 mA cm^{-2} was reached with an overpotential of 376 mV at the first cycle of LSV. Initially, the current density decreased with the number of HER cycles, and then gradually stabilized, especially for cycles 3–10. At −0.42 V vs RHE, a stable current of 15 mA cm^{-2} lasted over 9 h of testing (Figure 2b). As shown in Figure 2c, the Tafel slope is 114.6 mV dec^{-1}, implying the rate determination step should be the Volmer process.[35] The electrochemical impedance spectroscopy (EIS) results before and after the long-term HER measurement are shown in Figure 2d, which demonstrate that the charge transfer resistance (R_{ct}, represented by the diameter of the semicircle) decreased significantly after the testing, while the contact resistance (R_s) decreased slightly. This implies the HER catalytic activity of the sample increased significantly compared to the as-received sample.

The samples after the HER tests were collected and characterized to understand the mechanism of the observed HER performance. SEM analysis was carried out on the "1-LSV" (sample after the first LSV test), "10-LSV", and '9 h of stability' tested samples. A layer of nanoparticles with a mean particle diameter ≈90 nm on top of Ag foil were observed for the 1-LSV sample (**Figure 3**a). From the EDX analysis, only Ag was detected in the sample (inset of Figure 3a), and boron signal was not found. The sample was further characterized by XPS (Figure 3b), which also did not detect any boron signal. Boron signal is invisible in the EDX and XPS spectra, which indicates that boron must have been leached out from $Ag_2B_{12}H_{12}$ to the 0.5 M H_2SO_4 solution during HER.

$Ag_2B_{12}H_{12}$ is insoluble in water and in weak acidic solution.[21,34] In fact, SEM, Raman, and EDX analysis also confirm that the sample maintains its original chemical state and composition after being soaked in 0.5 M H_2SO_4 for 48 h. However, when nuclear magnetic resonance spectroscopy (NMR) was employed to monitor the ^{11}B signal in the H_2SO_4 solution after one LSV run, in the ^{11}B NMR spectrum a doublet (δ = 15.2 ppm, J_{BH} ≈125 Hz) was observed (Figure 3c), a typical fingerprint of the $[B_{12}H_{12}]^{2-}$ cluster.[36,37] This indicates that the cluster was leached to the solution during HER. This also confirms that the enhanced HER activity is related to the in situ generated Ag nanoparticles. It is noted that the observed high current density at the beginning of the first cycle of the LSV (within the 0.1 to 0 V vs RHE) in Figure 2a can be attributed to the rapid Ag^+ ion reduction to Ag (0) due to the weakly coordinating nature of $[B_{12}H_{12}]^{2-}$ cluster.[22,23] The initial high current density (within the 0.1 to 0 V vs RHE) was not observed in the subsequent LSV cycles, as most of the Ag^+ ions in $Ag_2B_{12}H_{12}$ were reduced to Ag (0) during the first LSV (Figure 2a). After 10 cycles of LSV, the morphology of the sample is very similar to that after the first cycle, but with an increased mean particle diameter of ≈135 nm (Figure 3a; Figure S4a, Supporting Information, respectively). Again, no boron was detected from the EDX spectra of the 10-LSV sample. The HER performance also improved from the 1st cycle of LSV and then stabilized till the 10th cycle. This could be due to the rapid formation of Ag (0) nanoparticles during the testing. During the stability test at 0.42 V, after ≈3.5 h, the HER performance became stable. After 9 h, Ag nanoparticles were still visible on top of the Ag surface (Figure S4b, Supporting Information), but with clear

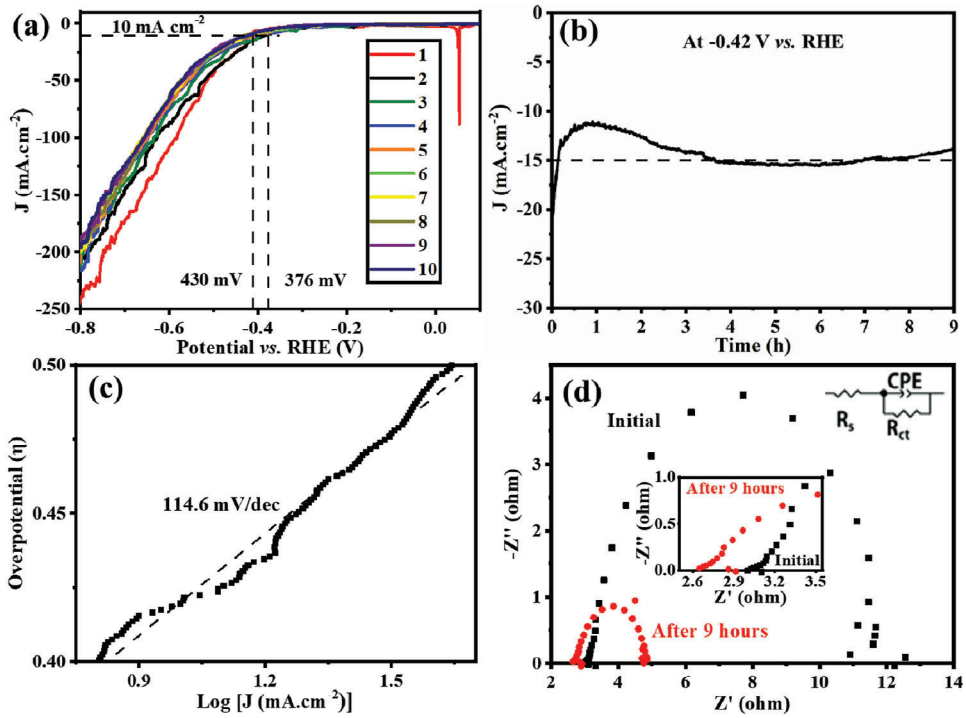

Figure 2. a) Linear sweep voltammetry (LSV) curves showing the HER performance of $Ag_2B_{12}H_{12}$ on Ag foils; b) stability test for the HER performance at −0.42 V vs RHE for 9 h; c) Tafel plots at a 10 mV s^{-1} scanning rate; d) Nyquist plots at the beginning and after 9 h of HER test. Inset is the magnified high frequency region and the electrical equivalent circuit of the 9 h tested sample.

agglomeration. Larger Ag nanoparticles (mean particle diameter ≈322 nm) can be distinguishable compared to the Ag nanoparticles after 1- and 10 -cycles of the LSV runs, respectively.

Additionally, in order to investigate the effects of the rate of both Ag electro-dissolution and Ag^+ electro-reduction on the formation of Ag catalysts, we conducted a CV treatment of Ag foil at different scan rates and compared the morphology of the Ag catalysts obtained. As shown in the SEM images (Figure S5, Supporting Information), the shape and size of the Ag nanoparticles obtained at different scan/redox rates are similar.

A comparison of the HER performance of various types of nano-Ag HER electrocatalysts is presented in Table S1 (Supporting Information). According to the previous reports, reduced particle size,[8,11,13] preferential facets of the Ag nanoparticles,[9] and stacking faults and defects inside Ag nanoparticles,[13] help to enhance the HER performance. In this work, only the particle size of the Ag nanoparticles was changed. The correlation between the high HER performance with the reduction in the Ag nanoparticle size is apparent, corroborating the results of the previous works.[8,9,11,13]

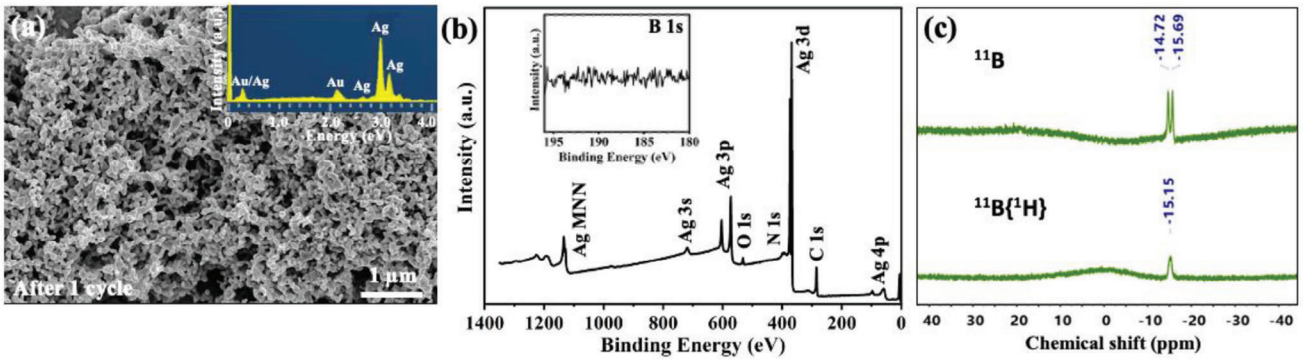

Figure 3. Characterization of the sample after the LSV tests. a) SEM image of the film after the first LSV. EDX analysis (shown in the inset) picks up only Ag; b) XPS spectrum confirms that boron is absent from the solid sample; c) ^{11}B NMR spectra show that $[B_{12}H_{12}]^{2-}$ is present in the solution after the LSV tests.

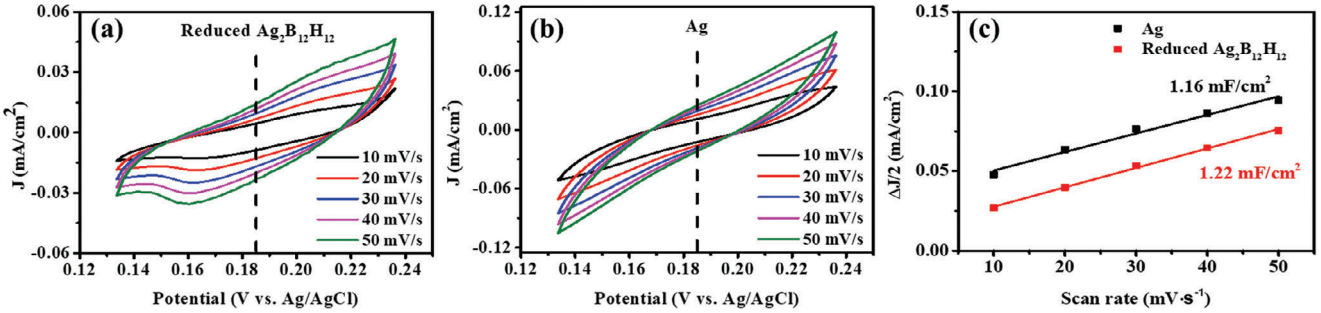

Figure 4. ECSA measurements. a,b) Cyclic voltammetry (CV) curves in the non-faradaic regions for the reduced $Ag_2B_{12}H_{12}$, and Ag, respectively. c) The linear relation of Δj/2 and scan rates for ECSA tests.

2.3. ECSA Analysis of $Ag_2B_{12}H_{12}$ Films on Ag Foils and Bare Ag Foil

To further evaluate the electrochemical activity of the reduced $Ag_2B_{12}H_{12}$ and Ag catalysts, the electrochemical specific surface area (ECSA) was calculated. As shown in **Figure 4**, the reduced $Ag_2B_{12}H_{12}$ possesses slightly larger electrochemical double-layer capacitance (C_{dl}) values compared to Ag foil. The ECSA of the reduced $Ag_2B_{12}H_{12}$ and Ag were determined to be 30.5, and 29 cm^{-2}, respectively, suggesting the slight enhancement of the ECSA by the smaller Ag nanoparticles and higher intrinsic activity of the reduced $Ag_2B_{12}H_{12}$ than Ag foil.

The total current densities from LSV curves of the two samples were normalized by the ECSA (Figure S6, Supporting Information), which are inversely proportional to the Ag particle sizes, confirming that the particle size plays an important role in determining the activity of Ag catalyst on HER.

2.4. HER Performance of the Annealed Ag2B12H12

To further prove that the HER activity originates from the freshly generated Ag nanoparticles, we annealed $Ag_2B_{12}H_{12}$ on Ag foils at high temperatures. It was reported that annealing $Ag_2B_{12}H_{12}$ above 320 °C produced metallic Ag and amorphous boron.[21] **Figure 5**a shows the SEM image of an as-synthesized $Ag_2B_{12}H_{12}$ particle and Figure 5b shows the SEM image of the annealed $Ag_2B_{12}H_{12}$ on Ag foil at 350 °C under 5% H_2 in Ar for 1 h. H_2 is necessary to prevent the oxidation of the sample at high temperatures. Octahedral $Ag_2B_{12}H_{12}$ particles containing Ag nanoparticles on the surfaces were found. The XRD pattern confirms that the $Ag_2B_{12}H_{12}$ phase no longer exists after the thermal treatment (Figure 5e). The broad peak at a low 2θ angle (14°) can be assigned to amorphous boron, while the sharp peaks are associated with Ag. Raman analysis was also carried out on the annealed samples. The B—H and B—B peaks that were readily seen in the as-prepared $Ag_2B_{12}H_{12}$ samples were absent in the annealed samples (Figure S7, Supporting Information). Since this annealing treatment generated large amounts of Ag nanoparticles, we expected this sample to be a good candidate for HER. Indeed, we obtained a decent HER performance from this sample, with a current density of 10 mA cm^{-2} at 395 mV overpotential (Figure 5f).

Annealing the sample at 450 °C for 1 h resulted in larger Ag particles around the original $Ag_2B_{12}H_{12}$ particles (Figure 5c), leading to the formation of the extended Ag network (Figure S8, Supporting Information). The corresponding HER performance also decreased due to the reduced surface area. At a higher temperature of 550 °C, the structure collapsed, as evidenced by the flat particles in Figure 5d, and Ag was mostly found surrounding the collapsed particle (Figure S9, Supporting Information). The XRD pattern of the sample only shows pure Ag metal peaks,

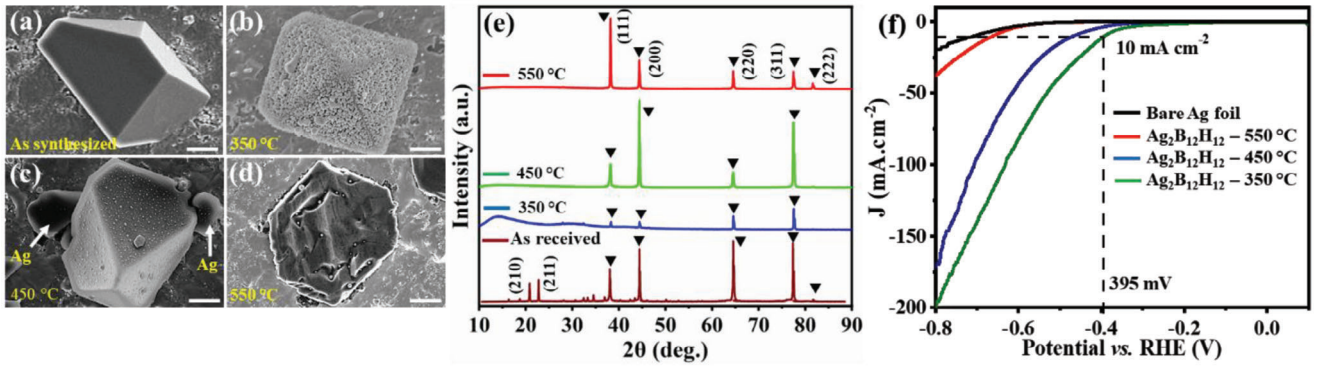

Figure 5. a) One as-synthesized $Ag_2B_{12}H_{12}$ particle on Ag foil; b–d) morphology of a representative $Ag_2B_{12}H_{12}$ particle after being annealed for 1 h at b) 350 °C; c) 450 °C, and d) 550 °C, respectively. The scale bar is 1 μm; e) XRD pattern of the as-synthesized and annealed samples. The black inverted triangles indicate the Ag metal peaks, matching with JCPDS, No. 04–0783. The rest of the peaks in the as-synthesized sample can be assigned to the $Ag_2B_{12}H_{12}$ phase. The high intensity peaks from (210) to (211) planes of $Ag_2B_{12}H_{12}$ appear at 20.31° and 22.28° 2θ angles, respectively; [21] f) LSV curves of a bare Ag foil and the annealed samples.

especially for the 550 °C annealed samples (Figure 5e), and the HER performance dropped significantly (Figure 5f). Correlating the Ag nanoparticle size with the observed HER performance for the electrochemically synthesized and annealed samples, it is clear that the larger Ag nanoparticles have lower HER performance.

3. Conclusion

In conclusion, we have demonstrated a new electrochemical route for the synthesis of $Ag_2B_{12}H_{12}$ film on Ag substrate. The crystallite size can be tuned by varying parameters such as voltage, current density, concentration, and time. When subjected to LSV test, Ag nanoparticles were formed due to Ag^+ ion reduction from $Ag_2B_{12}H_{12}$. Ag nanoparticles were also generated on the surfaces of $Ag_2B_{12}H_{12}$ film by annealing. In both cases, excellent HER activity was observed compared to bare Ag foil. The simple and effective electrochemical method is scalable and can be adopted to the syntheses of other metal *closo* dodecaborates. The in situ formation of Ag nanoparticles for HER sheds light on how to fabricate metal nanocatalysts electrochemically that can be used in various applications.

4. Experimental Section

Synthesis of $Ag_2B_{12}H_{12}$: The electrochemical synthesis of $Ag_2B_{12}H_{12}$ on Ag foil was carried out in 20 mM $Na_2B_{12}H_{12}$ aqueous solution using a standard three-electrode setup. A CHI electrochemical workstation was used to regulate the voltage and current. Pt was used as the counter electrode, and Ag/AgCl was used as the reference electrode. Ag foil (0.1 mm thick, purity 99.9%) was used as a working electrode that was first cleaned in acetone and sonicated for 5 min before the experiments. The influence of voltage, current, time of growth, and concentration of $Na_2B_{12}H_{12}$ on the size and morphology of $Ag_2B_{12}H_{12}$ was studied.

Annealing $Ag_2B_{12}H_{12}$: The thermal anneal of the as-synthesized $Ag_2B_{12}H_{12}$ film was carried out from 350 to 550 °C for 1 h, respectively, under a continuous flow of 5% H_2/Ar gas mixture inside a tubular furnace. H_2 was used to prevent sample oxidation during the reaction. Annealing was carried out by slowly ramping up (10 °C min^{-1}) to the desired temperature, holding at that temperature for 1 h, and then naturally cooling the sample to room temperature.

Characterization: Scanning electron microscopy (SEM) images and energy dispersive X-ray (EDX) spectra were obtained on Zeiss Supra 55 VP instrument. 1–5 kV operating voltage and <5 mm working distance were used to get the SEM images. EDX analysis was carried out at 5 kV. For imaging the $Ag_2B_{12}H_{12}$ thin films by SEM, a Leica EM ACE600 sputter coater was used to coat the sample with 5–10 nm of Au coating. Raman spectra of the samples were acquired using the 632.81 He-Ne laser source in a Renishaw Raman spectrometer. X-ray photoelectron spectroscopy (XPS) analysis was performed using the PHOIBOS 100 hemispherical analyzer and Al Kα as the X-ray source. Casa XPS software was used to analyze the XPS results. Data were calibrated using the C 1s peak position at 284.8 eV as a reference. ^{11}B NMR spectra were acquired on a Bruker Avance Neo 400 spectrometer at 298 K. X-ray diffraction (XRD) analysis was carried out on Bruker D8 Discover diffractometer. Cu Kα (wavelength = 1.54178 Å) X-ray source was used to test the sample at 40 kV and 40 mA voltage and current, respectively. Data were collected within the 5–90° 2θ range. A Dektan Stylus Profilometer was used to measure the $Ag_2B_{12}H_{12}$ film thickness on Ag foil.

Electrochemical Analysis: HER performance was evaluated by analyzing the linear sweep voltammetry (LSV) polarization curves of the samples. Graphite rod was used as the counter electrode. All the electrochemical potentials were expressed versus the reversible hydrogen electrode (RHE) potential. The LSVs were obtained from +0.1 to −0.8 V vs RHE, with a scan rate of 10 mV s^{-1} in 0.5 M H_2SO_4 solution. Nernst equation was used for the conversion of the potential to the RHE.

$$E_{RHE} = E_{Ag/AgCl} + 0.1976\ V + 0.0591 \times pH \quad (1)$$

The electrochemical impedance spectroscopy (EIS) measurement was performed with the three-electrode system in 1 M KOH solution, with the frequency ranging from 100 KHz to 0.1 Hz and an alternating current (AC) amplitude of 10 mV. The data were analyzed using ZView software. Tafel curves were obtained within 0.4 V to 0.5 V vs RHE overpotential.

Calculation of Electrochemically Active Surface Area (ECSA): The value of ECSA was calculated from the equation ECSA = C_{dl}/C_S. In the three-electrode system, the open circuit potential was determined to be ≈ 0.185 V vs Ag/AgCl. To measure the electrochemical double-layer capacitance (C_{dl}), CV curves at different scan rates (10, 20, 30, 40, and 50 mV s^{-1}) between 0.135 and 0.235 V were scanned in an H_2SO_4 solution (0.5 M). The differences in charging current density ($\Delta j/2 = |j_a - j_c|/2$) were plotted as a function of the scan rate. The C_{dl} was characterized by the slope of the fitted curve. According to the literature,[38] the general value of specific capacitance (C_S) was found to be 0.04 mF^{-2}_{ECSA}.

Supporting Information

Supporting Information is available from the Wiley Online Library or from the author.

Acknowledgements

Z.H. acknowledges support under the Australian Research Council's Discovery Projects funding scheme (project number DP220103458) and the Future Fellowship (FT190100658).

Open access publishing facilitated by University of Technology Sydney, as part of the Wiley - University of Technology Sydney agreement via the Council of Australian University Librarians.

Conflict of Interest

The authors declare no conflict of interest

Data Availability Statement

The data that support the findings of this study are available from the corresponding author upon reasonable request

Keywords

$Ag_2B_{12}H_{12}$, boron, hydrogen evolution reaction (HER), nanoparticles, silver

Received: June 18, 2023
Revised: October 30, 2023
Published online:

[1] J. D. Benck, T. R. Hellstern, J. Kibsgaard, P. Chakthranont, T. F. Jaramillo, *ACS Catal.* **2014**, *4*, 3957.
[2] N. Dubouis, A. Grimaud, *Chem. Sci.* **2019**, *10*, 9165.
[3] G. Zhao, K. Rui, S. X. Dou, W. Sun, *Adv. Funct. Mater.* **2018**, *28*, 1803291.

[4] J. Zhu, L. Hu, P. Zhao, L. Y. S. Lee, K.-Y. Wong, *Chem. Rev.* **2020**, *120*, 851.
[5] B. You, Y. Sun, *Acc. Chem. Res.* **2018**, *51*, 1571.
[6] X. Sun, W. Li, J. Chen, X. Yang, B. Wu, Z. Wang, B. Li, H. Zhang, *J. Colloid Interface Sci.* **2022**, *616*, 338.
[7] X. Zhao, M. Zheng, Z. Zhang, Y. Wang, Y. Zhou, X. Zhou, H. Zhang, *J. Mater. Chem. A* **2021**, *9*, 16427.
[8] J. Lu, J. Guo, S. Song, G. Yu, H. Liu, X. Yang, Z. Lu, *RSC Adv.* **2020**, *10*, 38583.
[9] T.-R. Kuo, Y.-C. Lee, H.-L. Chou, S. M. G, C.-Y. Wei, C.-Y. Wen, Y.-H. Chang, X.-Y. Pan, D.-Y. Wang, *Chem. Mater.* **2019**, *31*, 3722.
[10] Z. Liu, X. Wu, B. Zheng, Y. Sun, C. Hou, J. Wu, K. Huang, S. Feng, *Chem. Commun.* **2022**, *58*, 9890.
[11] W.-J. Kang, C.-Q. Cheng, Z. Li, Y. Feng, G.-R. Shen, X.-W. Du, *ChemCatChem* **2019**, *11*, 5976.
[12] M. A. Amin, S. A. Fadlallah, G. S. Alosaimi, *Int. J. Hydrogen Energy* **2014**, *39*, 19519.
[13] Z. Li, J.-Y. Fu, Y. Feng, C.-K. Dong, H. Liu, X.-W. Du, *Nat. Catal.* **2019**, *2*, 1107.
[14] Y. Jiao, Y. Zheng, M. Jaroniec, S. Z. Qiao, *Chem. Soc. Rev.* **2015**, *44*, 2060.
[15] J.-F. Huang, Y.-C. Wu, *ACS Sustainable Chem. Eng.* **2018**, *6*, 8285.
[16] M. N. Hossain, S. Ahmad, H.-B. Kraatz, *Int. J. Hydrogen Energy* **2021**, *46*, 2007.
[17] A. Bouafia, S. E. Laouini, A. S. A. Ahmed, A. V. Soldatov, H. Algarni, K. Feng Chong, G. A. M. Ali, *Nanomaterials* **2021**, *11*, 2318.
[18] J. Aihara, *J. Am. Chem. Soc.* **1978**, *100*, 3339.
[19] R. B. King, *Chem. Rev.* **2001**, *101*, 1119.
[20] J. Poater, C. Viñas, I. Bennour, S. Escayola, M. Solà, F. Teixidor, *J. Am. Chem. Soc.* **2020**, *142*, 9396.
[21] M. Paskevicius, B. R. S. Hansen, M. Jørgensen, B. Richter, T. R. Jensen, *Nat. Commun.* **2017**, *8*, 15136.
[22] T. Peymann, C. B. Knobler, S. I. Khan, M. F. Hawthorne, *J. Am. Chem. Soc.* **2001**, *123*, 2182.
[23] I. B. Sivaev, V. I. Bregadze, S. Sjöberg, *Collect. Czech. Chem. Commun.* **2002**, *67*, 679.
[24] H. Werheit, V. Filipov, U. Kuhlmann, U. Schwarz, M. Armbrüster, A. Leithe-Jasper, T. Tanaka, I. Higashi, T. Lundström, V. N. Gurin, M. M. Korsukova, *Sci. Technol. Adv. Mater.* **2010**, *11*, 023001.
[25] H. Hagemann, M. Sharma, D. Sethio, L. M. Lawson Daku, *Helv. Chim. Acta* **2018**, *101*, 1700239.
[26] V. V. Drozdova, E. A. Malinina, O. N. Belousova, I. N. Polyakova, N. T. Kuznetsov, *Russ. J. Inorg. Chem.* **2008**, *53*, 1024.
[27] K. U. Bareiß, S. Bette, D. Enseling, T. Jüstel, T. Schleid, *Dalton Trans.* **2022**, *51*, 13331.
[28] I. Tiritiris, J. Weidlein, T. Schleid, *Z. Naturforsch., B: J. Chem. Sci.* **2005**, *60*, 627.
[29] L. He, H.-W. Li, H. Nakajima, N. Tumanov, Y. Filinchuk, S.-J. Hwang, M. Sharma, H. Hagemann, E. Akiba, *Chem. Mater.* **2015**, *27*, 5483.
[30] B. R. S. Hansen, M. Paskevicius, H.-W. Li, E. Akiba, T. R. Jensen, *Coord. Chem. Rev.* **2016**, *323*, 60.
[31] J. F. Moulder, W. F. Stickle, P. E. Sobol, K. D. Bomden, *Handbook of X-ray Photoelectron Spectroscopy*, Perkin-Elmer Corporation, Minnesota, USA **1992**.
[32] B. Feng, J. Zhang, Q. Zhong, W. Li, S. Li, H. Li, P. Cheng, S. Meng, L. Chen, K. Wu, *Nat. Chem.* **2016**, *8*, 563.
[33] C. Hou, G. Tai, J. Hao, L. Sheng, B. Liu, Z. Wu, *Angew. Chem., Int. Ed.* **2020**, *132*, 10911.
[34] E. L. Muetterties, J. H. Balthis, Y. T. Chia, W. H. Knoth, H. C. Miller, *Inorg. Chem.* **1964**, *3*, 444.
[35] F. Bao, E. Kemppainen, I. Dorbandt, R. Bors, F. Xi, R. Schlatmann, R. Van De Krol, S. Calnan, *ChemElectroChem* **2021**, *8*, 195.
[36] V. Stavila, J.-H. Her, W. Zhou, S.-J. Hwang, C. Kim, L. A. M. Ottley, T. J. Udovic, *J. Solid State Chem.* **2010**, *183*, 1133.
[37] S. Hermanek, *Chem. Rev.* **1992**, *92*, 325.
[38] W. Li, J. Feng, Q. Xiong, H. Han, Z. Ma, *Sens. Actuators, B* **2023**, *393*, 134312.